NIH Public Access
Author Manuscript
Neuron. Author manuscript; available in PMC 2015 January 08.

Published in final edited form as:
Neuron. 2014 January 8; 81(1): 61–68. doi:10.1016/j.neuron.2013.10.031.

Pyramidal neurons in prefrontal cortex receive subtype-specific forms of excitation and inhibition

Anthony T. Lee[1,2,3,*], **Steven M. Gee**[1,2,3,*], **Daniel Vogt**[1], **John L. Rubenstein**[1], and **Vikaas S. Sohal**[1,2,3,†]

[1]Department of Psychiatry, University of California, San Francisco, 675 Nelson Rising Lane, San Francisco, CA 94143-0444

[2]Center for Integrative Neuroscience, University of California, San Francisco, 675 Nelson Rising Lane, San Francisco, CA 94143-0444

[3]Sloan-Swartz Center for Theoretical Neurobiology, University of California, San Francisco, 675 Nelson Rising Lane, San Francisco, CA 94143-0444

SUMMARY

Layer 5 pyramidal neurons comprise at least two subtypes: thick-tufted, subcortically-projecting Type A neurons, with prominent h-current, and thin-tufted, callosally-projecting Type B neurons, which lack prominent h-current. Using optogenetic stimulation, we find that these subtypes receive distinct forms of input that could subserve divergent functions. Repeatedly stimulating callosal inputs evokes progressively smaller excitatory responses in Type B but not Type A neurons. Callosal inputs also elicit more spikes in Type A neurons. Surprisingly, these effects arise via distinct mechanisms. Differences in the dynamics of excitatory responses reflect differences in presynaptic input, whereas differences in spiking depend on postsynaptic mechanisms. We also find that fast-spiking parvalbumin interneurons, but not somatostatin interneurons, preferentially inhibit Type A neurons, which leads to greater feedforward inhibition in this subtype. These differences may enable Type A neurons to detect salient inputs that are focused in space and time, while Type B neurons integrate across these dimensions.

INTRODUCTION

Patterns of network activity emerge from the organization of connections in neural circuits. Thus, it is critically important to determine whether these connections follow a specific wiring diagram, and if so, to identify possible computational functions that emerge as a result. Many studies have shown that across multiple neocortical regions, layer 5 (L5) pyramidal neurons can be divided into at least two subtypes (Brown and Hestrin, 2009; Dembrow et al., 2010; Gee et al., 2012; Hattox and Nelson, 2007; Morishima and Kawaguchi, 2006; Seong and Carter, 2012; Sheets et al., 2011; Wang et al., 2006). One subtype, which we call “Type A” neurons, has thick-tufted apical dendrites, projects subcortically, and has a prominent h-current (I_h). The other subtype – “Type B neurons” –

© 2013 Elsevier Inc. All rights reserved.

†Correspondence: vikaas.sohal@ucsf.edu.
*These two authors contributed equally to this work

Publisher's Disclaimer: This is a PDF file of an unedited manuscript that has been accepted for publication. As a service to our customers we are providing this early version of the manuscript. The manuscript will undergo copyediting, typesetting, and review of the resulting proof before it is published in its final citable form. Please note that during the production process errors may be discovered which could affect the content, and all legal disclaimers that apply to the journal pertain.

NIH-PA Author Manuscript
NIH-PA Author Manuscript
NIH-PA Author Manuscript

NIH-PA Author Manuscript

NIH-PA Author Manuscript

NIH-PA Author Manuscript

projects to the contralateral cortex or striatum, has thin tufted apical dendrites, and lacks prominent I_h.

Several groups have studied differences in local connections between these two subtypes (Brown and Hestrin, 2009; Morishima and Kawaguchi, 2006; Morishima et al., 2011; Wang et al., 2006). However, it remains unknown whether long-range excitatory inputs or local inhibitory connections also differ between these subtypes. Two recent studies found that neocortical interneurons nonspecifically target nearby pyramidal neurons (Fino and Yuste, 2011; Packer and Yuste, 2011) but these studies did not examine subtypes of L5 pyramidal neurons. By contrast, studies in other regions suggest that inhibitory interneurons can selectively innervate pyramidal neurons that project to specific targets, while sparing neighboring pyramidal neurons that project elsewhere (Krook-Magnuson et al., 2012; Varga et al., 2010).

To address these issues, we studies excitatory connections from the contralateral mPFC, and inhibitory connections from fast-spiking parvalbumin interneurons (FSINs) and somatostatin (SOM) interneurons onto Type A and B neurons in mPFC. We find that optogenetic stimulation of callosal inputs elicits distinct patterns of responses in Type A and B neurons and that FSINs preferentially innervate Type A neurons. These findings have important implications for the normal and pathological function of prefrontal microcircuits.

RESULTS

To compare responses of Type A and B neurons to callosal inputs, we performed dual whole cell recordings in pairs of Type A and B neurons while optogenetically stimulating inputs from the contralateral mPFC (n=11 pairs; Fig. 1A). We differentiated Type A and B neurons by the prominence of the I_h induced sag and rebound in response to hyperpolarizing current pulses and the presence of an afterhyperpolarization following depolarizing current pulses (Methods; Fig. S1A) (Gee et al., 2012). We expressed ChR2 in pyramidal neurons in the mPFC in one hemisphere (Methods; Fig. 1A), then stimulated the terminals of their callosal projections via rhythmic trains of light flashes (470nm; ~2 mW/mm^2, 5ms; 5 or 10 Hz, 10 flashes/train). Some studies optogenetically stimulate terminals in TTX + 4-AP to block polysynaptic activity (Petreanu et al., 2007). However, in TTX + 4-AP, synaptic release is triggered by the ChR2-driven depolarization of terminals rather than by spiking. This would not be suitable for studying the short-term dynamics of synaptic responses, therefore, by design, we did not use TTX + 4-AP to block polysynaptic activity. This also enabled us to measure how callosal inputs recruit different levels of spiking and feedforward inhibition in Type A and B neurons. We did attempt experiments using TTX + 4-AP, but found that optogenetically-evoked synaptic release was completely abolished (6/6 neurons; Fig. S1B), indicating that, in our preparation, optogenetically-evoked synaptic release is mediated by spiking. Although we could not use TTX + 4-AP to isolate monosynaptic responses, several observations described below suggest that monosynaptic callosal input dominated the responses we recorded.

Callosal stimulation elicits subtype-specific excitatory responses

Trains of optogenetic stimulation delivered to callosal inputs elicited EPSPs in Type A/B pairs. In 3/11 pairs, at least one cell spiked. In the remaining 8 pairs, all EPSPs were subthreshold. Notably, the pattern of subthreshold EPSPs differed in Type A and B neurons (Fig. 1B). We observed marked depression of subthreshold EPSP responses to successive light flashes in Type B neurons, i.e. the responses to light flashes 2–10 were consistently weaker than the first response ($p<0.001$ for an effect of response number on EPSP amplitude by ANOVA; EPSPs 2–10 were each weaker than the first EPSP, $p<0.05$ by t-test; n=8 cells). No such depression occurred in Type A neurons, and normalized EPSP responses to light

NIH-PA Author Manuscript

NIH-PA Author Manuscript

NIH-PA Author Manuscript

flashes 2–10 were significantly greater in Type A than Type B neurons ($p<10^{-4}$ for 5 Hz, $p<0.01$ for 10 Hz via ANOVA using cell subtype, recording pair, and flash number as factors; n=8 pairs; Fig. 1C). In fact, in some Type A neurons, the first few responses to light flashes at 5 Hz were facilitating, i.e. they grew progressively larger (gray traces in Fig. 1B). The average amplitude of the first EPSP was not significantly different in Type A and B neurons (p=0.18 for 5 Hz; p=0.41 for 10 Hz; n=8 pairs). To confirm that Type A and B neurons have different projection targets, we also made recordings after injecting fluorescent retrogradely transported microspheres (Lumafluor) into MD thalamus (red) and contralateral mPFC (green). In 3/3 pairs consisting of one corticothalamic (CT) and one corticocortical (CC) neuron, we observed the same pattern – strong depression of EPSPs in CC (Type B) neurons but not in CT (Type A) neurons (Fig. S1D–F).

Subtype-specific patterns of EPSPs could reflect differences in monosynaptic callosal inputs, or effects of polysynaptic activity. Three observations suggest that these differences arise at the level of monosynaptic callosal inputs. First, in all of the recordings used to analyze EPSPs, callosal stimulation failed to evoke spikes in either simultaneously recorded neuron, suggesting that in these recordings polysynaptic activity was limited. If one considers *all* recordings, including those in which we observed spiking, then on average, each neuron spikes in response to a light flash 7.5% of the time (there were 33 spikes in response to 440 light flashes, based on 22 cells, 2 sweeps per cell, and 10 light flashes per sweep). Of course, such an average obscures the fact that due to variable ChR2 expression across slices, a few experiments contained high levels of spiking while others contained minimal polysynaptic activity. Indeed, in 3 recordings, light stimulation failed to evoke appreciable inhibitory currents in either cell (measured in voltage clamp at +10 mV). These recordings presumably represent cases with the least ChR2 expression and minimal polysynaptic activity, but they still exhibit EPSP depression in Type B but not Type A neurons (Fig S1C). This represents a second line of evidence that differences in EPSPs arise at the level of monosynaptic inputs.

Finally, even when we did observe spiking (in current clamp), these spikes occurred 11.3 ± 1.7 msec after the light flash – well *after* the peak of the EPSC response, measured in voltage clamp (7.3 ± 0.5 msec after the light flash; n=6 cells). Thus, peak responses are likely to be dominated by monosynaptic input (though polysynaptic activity may also contribute). In summary, multiple factors suggest that differences in EPSP dynamics originate at the level of monosynaptic callosal inputs. Regardless, we have found that callosal inputs recruit distinct patterns of excitation in Type A and B neurons.

Differences in presynaptic input explain subtype-specific differences in EPSPs

We next asked whether the different EPSP dynamics in Type A and B neurons reflect pre- or postsynaptic mechanisms. When dual-patching onto A/B pairs in voltage clamp at −70 mV (Fig 2A, top), we did not find significant differences in peak excitatory currents or charge transfer (Fig 2B). Normalized, averaged excitatory currents elicited by light stimulation show that Type A or B neurons receive slightly facilitating or depressing currents, respectively (Fig 2C). We asked whether these facilitating and depressing currents suffice to reproduce the subtype-specific EPSP patterns in Fig. 1. This would suggest that subtype-specific patterns of presynaptic input account for differences in EPSP dynamics. Alternatively, different postsynaptic properties of Type A and B neurons, e.g. differences in resonance properties (Dembrow et al., 2010), may contribute to different EPSP responses. To address this, we averaged the input waveform recorded in voltage clamp from Type A neurons, and the waveform recorded from Type B neurons (Fig. 2C). Then we played back each waveform to both Type A and B neurons in current clamp (Fig. 2D). If cell-intrinsic properties contribute to differences in EPSP dynamics, voltage responses to the injected

NIH-PA Author Manuscript

NIH-PA Author Manuscript

NIH-PA Author Manuscript

inputs should depend on the identity of the patched neuron (A or B). However, the response of Type A and B neurons depended only on the identity of the injected current waveform (Fig 2E). Both Type A and B neurons showed EPSP depression in response to the "Type B" input waveform but not the "Type A" waveform (Fig 2F).

Of course, the current waveforms we recorded in voltage clamp may not accurately reflect synaptic input. These waveforms could be contaminated by unclamped dendritic currents in Type A and B neurons, and such voltage-dependent Ca^{2+} currents in the dendrites might enhance temporal summation between EPSPs in Type A neurons, masking the sort of EPSP depression observed in Type B neurons (Branco and Hausser, 2011; Schiller et al., 2000). To rule this out, we recorded Type A neuron responses to callosal stimulation before and after blocking T-type Ca^{2+} channels, L-type Ca^{2+} channels, and NMDARs with mibefradil (5 μM) + nimodipine (5 μM) + AP5 (50 μM). We found no alteration in the paired-pulse ratio after blocking these postsynaptic voltage-dependent Ca^{2+} channels (p=0.19, n=4, Fig S2), i.e. even after blocking these channels, EPSPs in Type A neurons were still non-depressing. This suggests that differences between the pattern of callosally-evoked EPSPs in Type A and B neurons reflect differences in their presynaptic input, not postsynaptic factors.

Differences in callosally-evoked spiking depend on postsynaptic Ca^{2+} currents

During paired-recordings of callosal stimulation (described above), we observed more spikes in Type A neurons than Type B neurons (Fig 3A; spiking occurred in 3/11 pairs; whereas we used 5–10 Hz trains to minimize ChR2 inactivation while studying EPSP depression, for studying spiking we used 20 Hz trains which led to greater EPSP summation and spiking). We asked whether greater Type A neuron spiking reflects differences in presynaptic inputs or postsynaptic excitability. To test this, we injected current waveforms resembling those in Fig 2C, but scaled up by a factor of 2 to elicit spikes. The waveforms in Fig. 2C reflect averages across all experiments, whereas EPSPs were larger in recordings that elicited spiking. Thus the "scaled up" waveforms were consistent with the EPSPs that elicited spiking. We also injected tonic current to maintain resting membrane potentials near −65 mV (neither the injected current nor the resulting resting potentials differed between type A and B neurons; resting potential, Type A: −65.7 ± 1.4 mV, Type B: −66.7 ± 0.3 mV, p=0.5; average current, Type A: 8.7 ± 4.1 pA, Type B: 15 ± 6.1 pA, p=0.4). Type A neurons spiked more than Type B neurons, regardless of whether we injected input waveforms derived from Type A or B neurons, suggesting that postsynaptic differences between Type A and B neurons contribute to differences in spiking (Fig 3B, C).

We have previously found that Ca^{2+} and Ca^{2+}-dependent currents profoundly influence the excitability of Type A neurons (Gee et al., 2012). To test whether similar mechanisms might enhance Type A neuron spiking here, we recorded the voltage responses of Type A neurons to input waveforms derived from both Type A and B neurons before and after applying Ni^{2+} (0.5 mM) to block voltage-gated Ca^{2+} channels. The increased firing observed in Type A neurons was significantly reduced when voltage-gated calcium channels were blocked ($p<0.01$; Fig 3B–D), suggesting that voltage-gated Ca^{2+}channels contribute to increased spiking in Type A neurons.

We also tested whether the more prominent I_h in Type A neurons affects their responses to these input waveforms, but found minimal changes in spiking and EPSP dynamics after blocking I_h with ZD7288 (25 μM; Fig. S3).

Callosal stimulation elicits more circuit inhibition in Type A neurons

Excitatory callosal inputs recruit local feedforward inhibitory circuits. Thus we tested if Type A and B neurons receive different levels of feedforward inhibition. In the previously

NIH-PA Author Manuscript

NIH-PA Author Manuscript

NIH-PA Author Manuscript

described experiments, in which we excited ChR2-expressing callosal projections while dual-patching Type A and B neurons, we also recorded IPSCs in voltage-clamp at +10mV. Surprisingly, Type A neurons received significantly more inhibitory current than Type B neurons (Fig 4A, B). Both the peak IPSC amplitude (Type A: 1.0 ± 0.3 nA, Type B: 0.4 ± 0.2 nA; $p<0.01$) and inhibitory charge transfer (Type A: 18.9 ± 6.0 pC, Type B: 10.5 ± 5.5 pC; $p<0.05$) were significantly greater in Type A than B neurons (n=11 pairs). Fast outward currents were completely blocked by picrotoxin (10 μM; n=3; Fig. S4A). The latency from the beginning of each light flash to the peak of the IPSC was ~2ms ec longer than the corresponding latency for EPSCs (9.7 ± 0.8 msec vs. 7.3 ± 0.5 ms; Fig S4D), consistent with primarily feedforward (as opposed to feedback) inhibition.

Fast-spiking parvalbumin interneurons preferentially inhibit Type A neurons

Differences in inhibition might reflect different connectivity between inhibitory interneurons (INs) and these two pyramidal neuron subtypes. To explore this possibility, we recorded from fast-spiking parvalbumin interneurons (FSINs) in current clamp while simultaneously recording from either Type A or B neurons in voltage clamp at +10mV (Fig 4C). We initially selected putative INs based on expression of mCherry driven by an AAV with the DlxI12b enhancer (Methods) (Potter et al., 2009), then confirmed FSIN identity based on electrophysiological criteria (Methods). FSINs had significantly greater probabilities of connecting onto Type A than Type B neurons (6/11 vs 1/12, $p=0.027$, Fisher's exact test). Importantly, the average distance between FSINs and Type A or B neurons was not significantly different (Fig. S4E).

To further investigate inhibitory output from FSINs onto different L5 pyramidal neuron subtypes, we optogenetically activated FSINs while simultaneously recording from a pair of Type A and B neurons. We injected AAV to drive Cre-dependent ChR2 expression into the mPFC of parvalbumin (PV)::Cre mice (Sohal et al., 2009) (Fig 4E), in which Cre expression is limited to PV-positive INs, which in neocortex are FSINs. Optogenetic stimulation of PV INs elicited significantly greater peak inhibitory current (Type A: 2.6 ± 0.7 nA; Type B: 1.3 ± 0.5 nA, $p<0.05$) and charge transfer (Type A: 60 ± 16 pC; Type B: 36 ± 13 pC, $p<0.01$) in Type A compared to Type B neurons. Again, we confirmed that this pattern of greater inhibition in Type A neurons was also present in pairs of retrogradely-labeled CT/CC neurons (data not shown; n=2 pairs).

Finally, to determine whether this preferential inhibition of Type A neurons was specific to FS/PV INs, we also recorded from pairs of Type A and B neurons in somatostatin (SOM)::Cre mice injected with the same AAV (Fig. S4F). In this case, we evoked inhibition by stimulating ChR2 in SOM INs, and found no consistent difference between peak inhibitory currents (Type A: 1.2 ± 0.3 nA; Type B: 1.0 ± 0.3 nA, $p=0.6$) or inhibitory charge transfer in Type A and B neurons (Type A: 37 ± 10 pC; Type B: 34 ± 10 pC, $p=0.8$) (Fig. S4F–G).

Inhibition sharpens Type A neuron responses to callosal input

If callosal inputs preferentially recruit feedforward inhibition in Type A neurons, this may accelerate the return to baseline following EPSPs in Type A neurons. We revisited our current clamp traces (Fig 1B) and calculated the decay time constant for the falling phase of EPSPs (Fig 4G). Indeed, Type A neurons had sharper responses to callosal inputs as indicated by their significantly shorter decay time constant (Fig 4H, Type A: 41 ± 7 ms; Type B: 92 ± 19 ms, $p<0.05$).

Feedforward inhibition might also influence the facilitation or depression of EPSPs in Type A neurons. To test this, we recorded EPSPs in Type A neurons before and after applying

NIH-PA Author Manuscript

NIH-PA Author Manuscript

NIH-PA Author Manuscript

picrotoxin (PTX) to block $GABA_A$ currents. To avoid epileptiform discharges we applied 10 μM PTX for 10–16 min. While this eliminated most feedforward IPSCs (Fig. S4A), PTX had minimal effects on the facilitation or depression of Type A neuron EPSPs (Fig. S4B–C). However, PTX did significantly prolong the decay time constant of Type A neuron EPSPs (from 29 ± 6 msec to 45 ± 8 msec; Fig. S4A; n=4 cells; $p<0.001$ by repeated measures ANOVA), confirming that inhibition sharpens Type A neuron responses to callosal input.

DISCUSSION

These results build on earlier studies that divided L5 pyramidal neurons in the mPFC into two subtypes. We found that callosal inputs elicit depressing EPSPs in Type B neurons while EPSPs both fail to depress and evoke more spikes in Type A neurons. Differences in the dynamics of EPSPs can be explained by differences in presynaptic inputs to Type A and B neurons whereas postsynaptic differences, including voltage-dependent Ca^{2+} currents in Type A neurons, drive the higher level of spiking in these neurons. Several observations suggest these differences derive primarily from monosynaptic callosal inputs. In particular, these differences are present even when polysynaptic activity is minimal (indicated by the absence of evoked inhibition). Regardless, callosal input elicits excitatory circuit activity that manifests differently in Type A and B neurons. Callosal inputs also elicit approximately twice as much circuit inhibition in Type A neurons compared to Type B neurons. We found that FSINs (but not SOM INs) preferentially innervate Type A neurons, which may explain this difference.

Relationship to previous studies

Previous studies have found differences in local connections between subtypes of L5 pyramidal neurons (Brown and Hestrin, 2009; Morishima and Kawaguchi, 2006; Morishima et al., 2011; Wang et al., 2006). Our findings suggest that similar differences are also present for long-range inputs, in this case, from the contralateral mPFC. Notably, callosal stimulation elicits EPSPs which depress in Type B but not Type A neurons, consistent with previous findings that local excitatory connections between neurons resembling either Type A or B neurons exhibit facilitation and depression, respectively (Morishima et al., 2011; Wang et al., 2006).

Our result that FSINs preferentially inhibit Type A neurons may explain an earlier observation that disynaptic inhibition occurs more frequently between pairs of thick-tufted L5 pyramidal neurons than between pairs of callosally projecting L5 pyramidal neurons (Le Be et al., 2007). However, our result contrasts with an older anatomical study in cat visual cortex, showing that corticocortical neurons receive more inhibitory synapses onto their somata and axon initial segments than do corticothalamic neurons (Farinas and DeFelipe, 1991). It will be important to determine whether this reflects species or regional differences, or differences between anatomical and physiologic measurements.

Our finding of differential FSIN output onto neighboring subtypes of L5 pyramidal neurons parallels similar findings in entorhinal cortex (Varga et al., 2010), but contrasts with another study of neocortical FSINs (Packer and Yuste, 2011). There are several differences between the latter study and this one, including the methods for measuring interneuron connectivity (glutamate uncaging vs. paired recording), ages (P12–17 vs. adult), neocortical regions (primarily somatosensory vs. prefrontal), and layers studied (primarily L2/3 vs. L5). It will be important to determine which factors explain the differences between these studies.

NIH-PA Author Manuscript

NIH-PA Author Manuscript

NIH-PA Author Manuscript

Implications for normal and pathological prefrontal microcircuit function

Increased circuit inhibition in Type A neurons, likely mediated by increased FSIN innvervation, sharpens Type A neuron responses to callosal input. By contrast, the relative absence of such inhibition results in an approximate doubling of EPSP duration in Type B neurons, which could enhance temporal summation. These differences could act in concert with differences in EPSP facilitation or depression to render Type A and B neurons maximally sensitive to distinct patterns of input. Specifically, if inputs to Type A neurons facilitate even weakly, then Type A neurons will respond more when inputs are concentrated on a single fiber, eliciting facilitation, than when inputs are distributed across many fibers, in which case no facilitation occurs. Depressing inputs elicit the opposite pattern: input concentrated on a single fiber cause depression, and as a consequence, Type B neurons should respond more strongly when inputs are distributed across many fibers. These differences may endow Type A and B neurons with distinct computational properties. Specifically, Type B neurons, which project callosally, may integrate intracortical signals from many input fibers over time to accumulate evidence as part of decision making (Curtis and Lee, 2010), or maintain persistent activity that stores items in working memory (Funahashi et al., 1989). By contrast, Type A neurons may be sensitive to strong, focal inputs that are concentrated onto a small number of input fibers and occur close together in time. This may enable Type A neurons to transmit signals about particularly salient events to downstream subcortical structures, e.g. MD thalamus, as part of corollary discharge (Wang et al., 2004). Activation of dopamine D2 receptors may further amplify Type A neuron responses to salient inputs (Gee et al., 2012).

Greater FSIN innervation of Type A neurons suggests that FSIN dysfunction, hypothesized to play a major roles in schizophrenia (Lewis et al., 2005), may cause relatively more severe disruptions in Type A neuron function. Within prefrontal cortex, Type A neurons represent a point of convergence for FSIN-mediated inhibition, L-type Ca^{2+} channels, outputs to MD thalamus, and D2 receptors, all of which have been strongly linked to schizophrenia (Marenco et al., 2012; Ripke et al., 2011). Thus, abnormal Type A neuron excitability may represent a specific physiological substrate that contributes to prefrontal dysfunction in schizophrenia.

Limitations and future directions

Although we recorded simultaneous responses of Type A and B neurons to callosal inputs, we do not know whether the same callosal fibers synapsed onto both Type A and B neurons, or whether subpopulations of callosal fibers, originating from different neurons, innervate these two subtypes. Future experiments might selectively stimulate various subpopulations of callosally-projecting prefrontal neurons, while measuring the responses of Type A and B neurons to disambiguate these two possibilities.

Conclusions

Callosal inputs elicit circuit excitation and inhibition that manifest differently in two subtypes of L5 pyramidal neurons within the mPFC, possibly contributing to distinct computational functions. It will be important for future studies to determine whether other long-range inputs also differentially innervate these and other subtypes of prefrontal neurons.

EXPERIMENTAL PROCEDURES

All experiments were conducted in accordance with procedures established by the Administrative Panels on Laboratory Animal Care at the University of California, San Francisco.

NIH-PA Author Manuscript

NIH-PA Author Manuscript

NIH-PA Author Manuscript

Slice preparation

We cut 250 μm coronal slices from 8–11 week-old mice of either sex (Gee et al., 2012). Slices were cut in a chilled slicing solution in which Na^+ was replaced by sucrose, then incubated in warmed ACSF at 30–31 degC for ~1 hour before being used for recordings. ACSF contained (in mM): 126 NaCl, 26 $NaHCO_3$, 2.5 KCl, 1.25 NaH_2PO_4, 1 $MgCl_2$, 2 CaCl, and 10 glucose. We used the following mouse lines: wild-type C57BL/6 mice (Charles River), B6;129P2--*Pvalb*$^{tm1(cre)Arbr}$/J (Jackson Labs), and B6N.Cg-Sst$^{tm2.1(cre)Zjh}$/J (Jackson Labs). We secured the slice via a harp along the midline.

Intracellular recording

We obtained somatic whole-cell patch recordings from visually identified pyramidal cells in layer 5 infralimbic or prelimbic cortex using differential contrast video microscopy on an upright microscope (BX51WI; Olympus). Recordings were made using a Multiclamp 700A (Molecular Devices). Patch electrodes (tip resistance = 2–6 MOhms) were filled with the following (in mM): 130 K-gluconate, 10 KCl, 10 HEPES, 10 EGTA, 2 MgCl, 2 MgATP, and 0.3 NaGTP (pH adjusted to 7.3 with KOH). All recordings were at 32.5±1°C. Series resistance was usually 10–20 MΩ, and experiments were discontinued above 30 MΩ.

Injection of virus for ChR2 expression

For Cre-dependent expression of ChR2 or EFYP, we used a previously described adeno-associated virus (AAV) vector that drives Cre-dependent expression of a ChR2-EFYP fusion protein (Sohal et al., 2009). In other cases, we expressed ChR2-EFYP in pyramidal neurons using a previously described AAV vector that contains a gene encoding ChR2-EYFP under control of the promoter for CaMKIIα (Sohal et al., 2009). In each case, we injected 0.5–0.75 μl of virus following previously described procedures (Sohal et al., 2009). For experiments in which we recorded from ChR2-negative neurons while stimulating ChR2-positive axons, we injected virus into the contralateral medial PFC (mPFC), and verified that we observed fluorescent soma on the injected side, but not on the contralateral side (which was the location for recording). For experiments where we recorded from pyramidal neuron-interneuron pairs, we injected Cre-dependent ChR2-EYFP virus into ipsilateral mPFC. We waited at least 4 weeks after virus injection before preparing brain slices. Coordinates for injection into mPFC were (in millimeters relative to bregma): 1.7 anterior-posterior (AP), 0.3 mediolateral (ML), and −2.75 dorsoventral (DV).

Injection of retrogradely transported microspheres for projection targeting experiments

Procedures for injection of these microspheres were similar to those for virus injection. We waited at least 48 h after each injection before preparing brain slices. Coordinates for mPFC injections were the same as for virus injections. For injections into mediodorsal (MD) thalamus, coordinates were (in millimeters relative to bregma): +1.7 AP, 0.3 ML, and −3.5 DV. For each experiment, we verified that microspheres were present in the correct target (MD thalamus or mPFC). For injections into MD thalamus we also verified that microspheres were not present in neighboring structures, e.g. striatum.

Electrophysiological identification of Type A neurons

Type A neurons were distinguished by their voltage sag and rebound afterdepolarization (ADP) following hyperpolarizing current pulses (−200 pA, 250 msec), and afterhyperolarization (AHP) following depolarizing current pulses (250 pA, 250 msec): Type A neurons were defined based on a combined sag, rebound ADP, and AHP >6.5 mV.

NIH-PA Author Manuscript

NIH-PA Author Manuscript

NIH-PA Author Manuscript

Electrophysiologic identification of fast spiking interneurons

Fast-spiking interneurons were first preliminarily identified through an AAV-Dlxi12b enhancer-mCherry, which marks a diverse population of interneurons (Potter et al., 2009). Putative interneurons were then identified as fast-spiking based on electrophysiological properties. Specifically, the action potential width at half-maximal amplitude was ≤0.5 msec, and during responses to a depolarizing current pulse (400 pA, 250 msec), the adaptation ratio, i.e. the ratio between the first and last interspike interval was <2.

Drug application

For electrophysiology, all drugs were dissolved in water (DL-AP5, 4AP, bicuculline methiodide, ZD7288) or dimethylsulfoxide (mibefradil, nimodipine, nickel, picrotoxin) before being diluted in ACSF, except for tetrodotoxin (TTX), which was dissolved in a pH 4.8 citrate buffer.

ChR2 stimulation

We stimulated ChR2 using flashes of light (~2mW/mm^2 measured at the sample) generated by a Lambda DG-4 high-speed optical switch with a 300W Xenon lamp (Sutter Instruments), and an excitation filter set centered around 470 nm, delivered to the slice through a 40x objective (Olympus). Illumination was delivered across a full high-power (40x) field. We delivered 5 Hz trains of light flashes first, followed by 10 Hz and 20 Hz trains. The interval between each train was at least 8 sec.

Statistical analysis

We used Student's t-tests to compare pairs of groups, unless there were repeated measurements or more than 2 groups, in which case we used ANOVA. In one case, as noted in the text, we used Fisher's exact test to compare the frequency of connections between two groups. Error bars indicate ± 1 SEM unless otherwise specified.

Supplementary Material

Refer to Web version on PubMed Central for supplementary material.

Acknowledgments

This work was supported by the Staglin Family, International Mental Health Research Organization, NIMH (R00MH085946), Simons Foundation for Autism Research, Alfred P. Sloan Foundation, and NIH Office of the Director (DP2MH100011). In addition, JLR is supported by NIMH (R37MH049428), and ATL by a Medical Scientist Training Grant from NIGMS (GM07618).

References

Branco T, Hausser M. Synaptic integration gradients in single cortical pyramidal cell dendrites. Neuron. 2011; 69:885–892. [PubMed: 21382549]

Brown SP, Hestrin S. Intracortical circuits of pyramidal neurons reflect their long-range axonal targets. Nature. 2009; 457:1133–1136. [PubMed: 19151698]

Curtis CE, Lee D. Beyond working memory: the role of persistent activity in decision making. Trends Cogn Sci. 2010; 14:216–222. [PubMed: 20381406]

Dembrow NC, Chitwood RA, Johnston D. Projection-specific neuromodulation of medial prefrontal cortex neurons. J Neurosci. 2010; 30:16922–16937. [PubMed: 21159963]

Farinas I, DeFelipe J. Patterns of synaptic input on corticocortical and corticothalamic cells in the cat visual cortex. I. The cell body. J Comp Neurol. 1991; 304:53–69. [PubMed: 2016412]

Fino E, Yuste R. Dense inhibitory connectivity in neocortex. Neuron. 2011; 69:1188–1203. [PubMed: 21435562]

NIH-PA Author Manuscript NIH-PA Author Manuscript NIH-PA Author Manuscript

Funahashi S, Bruce CJ, Goldman-Rakic PS. Mnemonic coding of visual space in the monkey's dorsolateral prefrontal cortex. J Neurophysiol. 1989; 61:331–349. [PubMed: 2918358]

Gee S, Ellwood I, Patel T, Luongo F, Deisseroth K, Sohal VS. Synaptic activity unmasks dopamine D2 receptor modulation of a specific class of layer V pyramidal neurons in prefrontal cortex. J Neurosci. 2012; 32:4959–4971. [PubMed: 22492051]

Hattox AM, Nelson SB. Layer V neurons in mouse cortex projecting to different targets have distinct physiological properties. J Neurophysiol. 2007; 98:3330–3340. [PubMed: 17898147]

Krook-Magnuson E, Varga C, Lee SH, Soltesz I. New dimensions of interneuronal specialization unmasked by principal cell heterogeneity. Trends Neurosci. 2012; 35:175–184. [PubMed: 22119146]

Le Be JV, Silberberg G, Wang Y, Markram H. Morphological, electrophysiological, and synaptic properties of corticocallosal pyramidal cells in the neonatal rat neocortex. Cereb Cortex. 2007; 17:2204–2213. [PubMed: 17124287]

Lewis DA, Hashimoto T, Volk DW. Cortical inhibitory neurons and schizophrenia. Nat Rev Neurosci. 2005; 6:312–324. [PubMed: 15803162]

Marenco S, Stein JL, Savostyanova AA, Sambataro F, Tan HY, Goldman AL, Verchinski BA, Barnett AS, Dickinson D, Apud JA, et al. Investigation of anatomical thalamo-cortical connectivity and FMRI activation in schizophrenia. Neuropsychopharmacology. 2012; 37:499–507. [PubMed: 21956440]

Morishima M, Kawaguchi Y. Recurrent connection patterns of corticostriatal pyramidal cells in frontal cortex. J Neurosci. 2006; 26:4394–4405. [PubMed: 16624959]

Morishima M, Morita K, Kubota Y, Kawaguchi Y. Highly differentiated projection-specific cortical subnetworks. J Neurosci. 2011; 31:10380–10391. [PubMed: 21753015]

Packer AM, Yuste R. Dense, unspecific connectivity of neocortical parvalbumin-positive interneurons: a canonical microcircuit for inhibition? J Neurosci. 2011; 31:13260–13271. [PubMed: 21917809]

Petreanu L, Huber D, Sobczyk A, Svoboda K. Channelrhodopsin-2-assisted circuit mapping of long-range callosal projections. Nat Neurosci. 2007; 10:663–668. [PubMed: 17435752]

Potter GB, Petryniak MA, Shevchenko E, McKinsey GL, Ekker M, Rubenstein JL. Generation of Cre-transgenic mice using Dlx1/Dlx2 enhancers and their characterization in GABAergic interneurons. Mol Cell Neurosci. 2009; 40:167–186. [PubMed: 19026749]

Ripke S, Sanders AR, Kendler KS, Levinson DF, Sklar P, Holmans PA, Lin DY, Duan J, Ophoff RA, Andreassen OA, et al. Genome-wide association study identifies five new schizophrenia loci. Nat Genet. 2011; 43:969–976. [PubMed: 21926974]

Schiller J, Major G, Koester HJ, Schiller Y. NMDA spikes in basal dendrites of cortical pyramidal neurons. Nature. 2000; 404:285–289. [PubMed: 10749211]

Seong HJ, Carter AG. D1 receptor modulation of action potential firing in a subpopulation of layer 5 pyramidal neurons in the prefrontal cortex. J Neurosci. 2012; 32:10516–10521. [PubMed: 22855801]

Sheets PL, Suter BA, Kiritani T, Chan CS, Surmeier DJ, Shepherd GM. Corticospinal-specific HCN expression in mouse motor cortex: Ih-dependent synaptic integration as a candidate microcircuit mechanism involved in motor control. J Neurophysiol. 2011

Sohal VS, Zhang F, Yizhar O, Deisseroth K. Parvalbumin neurons and gamma rhythms enhance cortical circuit performance. Nature. 2009; 459:698–702. [PubMed: 19396159]

Varga C, Lee SY, Soltesz I. Target-selective GABAergic control of entorhinal cortex output. Nat Neurosci. 2010; 13:822–824. [PubMed: 20512133]

Wang M, Vijayraghavan S, Goldman-Rakic PS. Selective D2 receptor actions on the functional circuitry of working memory. Science. 2004; 303:853–856. [PubMed: 14764884]

Wang Y, Markram H, Goodman PH, Berger TK, Ma J, Goldman-Rakic PS. Heterogeneity in the pyramidal network of the medial prefrontal cortex. Nat Neurosci. 2006; 9:534–542. [PubMed: 16547512]

NIH-PA Author Manuscript

NIH-PA Author Manuscript

NIH-PA Author Manuscript

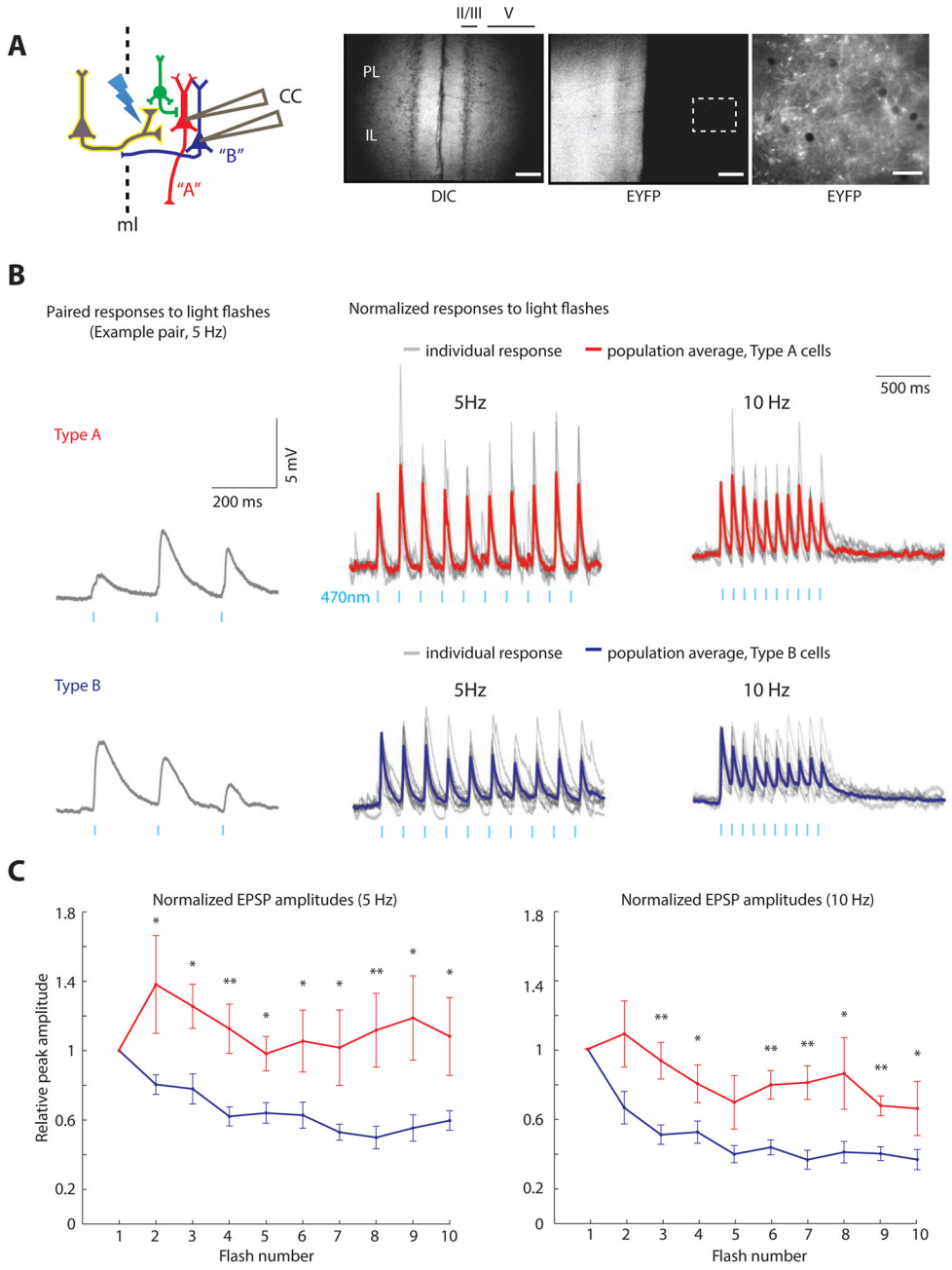

FIGURE 1. EPSP dynamics differ across subtypes of L5 pyramidal neurons

A) Experimental design: we simultaneously recorded from a Type A (red) and Type B (blue) pyramidal neuron while activating ChR2-expressing inputs (yellow) from the contralateral mPFC. Low-power images of mPFC, including the prelimbic and infralimbic cortices (PL and IL), showing a DIC image (left) and ChR2-EYFP expression (middle) (scale bar=50 μm). Right: High-power image of the dotted region in the middle panel, showing ChR2-EYFP expression in axon terminals from the contralateral mPFC (scale bar=12.5 μm). **(B)** Paired responses of Type A and B neurons to 5 Hz light stimulation in current clamp (left). Population average (bold) and individual (gray) current clamp responses to 5 Hz (middle) and 10 Hz (right) stimulation. **(C)** Normalized EPSP amplitudes

during trains of light flashes in Type A and B neurons with subthreshold responses (n=8/11 pairs). *=p<0.05, **=p<0.01. See also Figure S1.

NIH-PA Author Manuscript
NIH-PA Author Manuscript
NIH-PA Author Manuscript

NIH-PA Author Manuscript

NIH-PA Author Manuscript

NIH-PA Author Manuscript

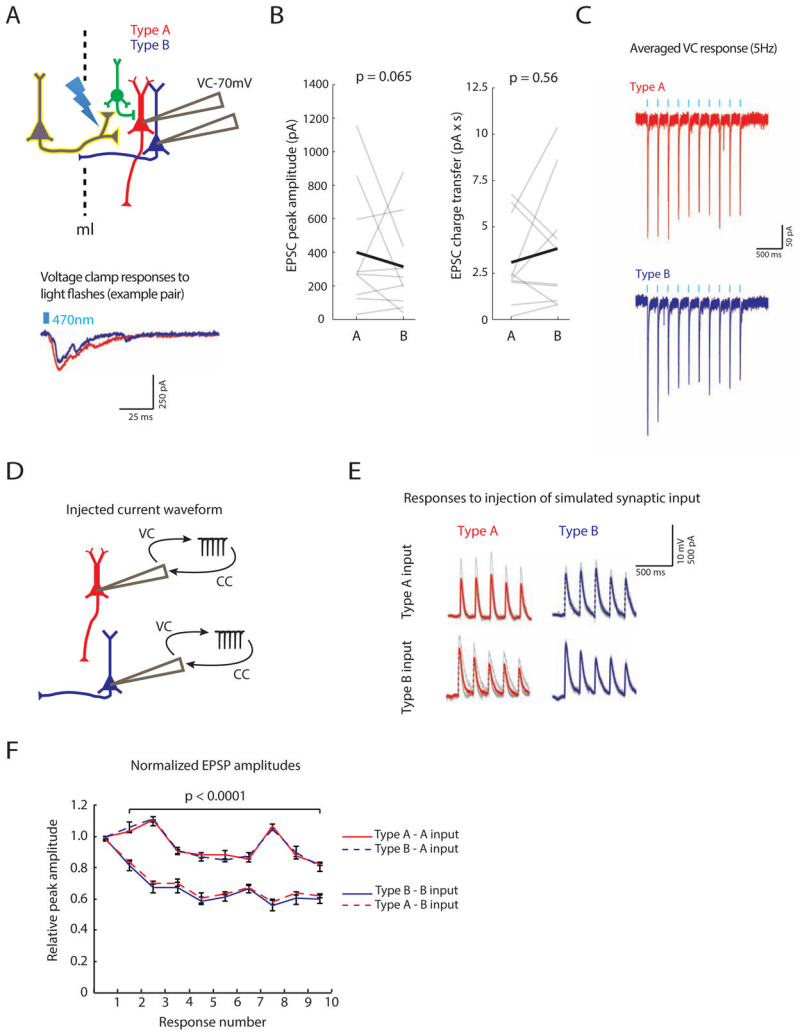

FIGURE 2. Subtype-specific synaptic responses in L5 pyramidal cells depend on presynaptic inputs

(A) Top: simultaneous recordings were made from Type A (red) and B (blue) neurons in voltage clamp at −70 mV while optogenetically stimulating callosal inputs (yellow). Example voltage traces from a Type A/B pair (bottom). **(B)** EPSC peak amplitude (left) and charge transfer (right) for each cell type**. (C)** Normalized, averaged voltage clamp responses to 5 Hz light stimulation in Type A (red) and B (blue) neurons (n=11 pairs). **(D)** Normalized, averaged voltage clamp responses of Type A and B neurons to callosal input were played back in current clamp to Type A or B neurons. **(E)** Population (bold) and individual (gray) current clamp responses to these averaged waveforms representing callosal inputs to either Type A or B neurons. **(F)** Normalized EPSP amplitudes in response to injection of Type A or B waveforms (n=4 for each condition). See also Fig. S2.

NIH-PA Author Manuscript

NIH-PA Author Manuscript

NIH-PA Author Manuscript

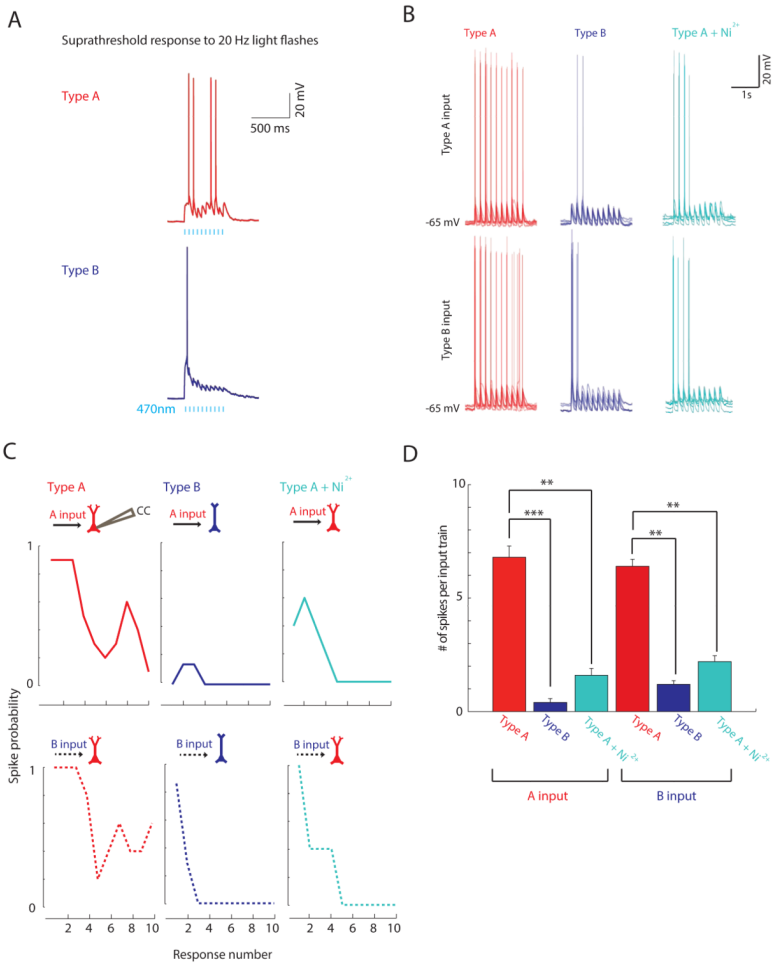

FIGURE 3. Postsynaptic Ca^{2+} currents contribute to increased spiking in Type A neurons

(A) Example of paired Type A/B responses illustrating greater spiking in Type A neurons. **(B)** Population overlay of responses of either Type A (red) or B (blue) neurons to Type A or B current waveforms. Type A neuron responses in Ni^{2+} are in teal. Steady current was injected to maintain all resting membrane potentials around −65 mV. **(C)** Spike probability for each simulated light pulse during injection of Type A or B current waveforms into postsynaptic Type A or B neurons. Type A neurons spiked more, regardless of the type of input waveform (A vs. B). Ni^{2+} dramatically reduces spiking in Type A neurons. **(D)** Number of spikes per train of ten simulated inputs. **=p<0.01, ***=p<0.001, n=5 for each condition. See also Fig. S3.

NIH-PA Author Manuscript

NIH-PA Author Manuscript

NIH-PA Author Manuscript

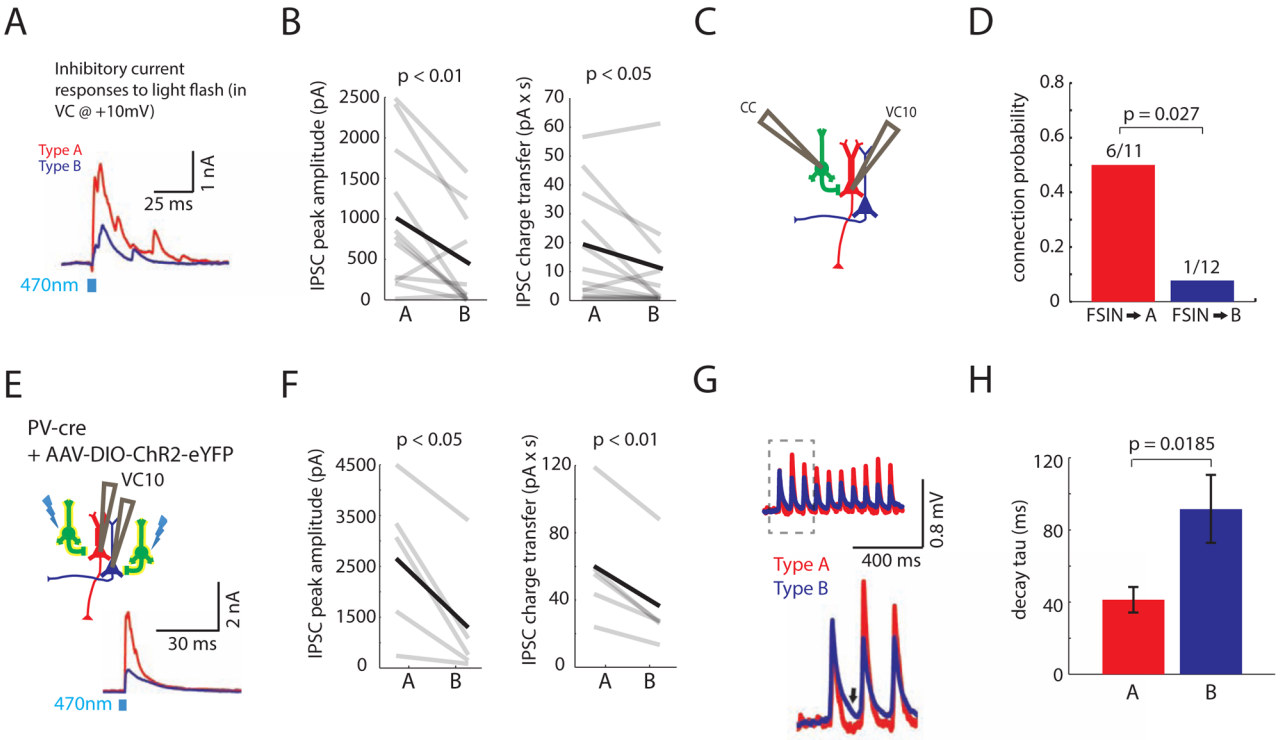

FIGURE 4. Fast-spiking parvalbumin interneurons preferentially inhibit Type A neurons

(A) Simultaneous recordings of IPSCs in a Type A and B neuron during optogenetic stimulation of callosal inputs. Cells were voltage clamped at +10mV. **(B)** Peak IPSC amplitude (left) and inhibitory charge transfer (right) were larger in Type A neurons compared to simultaneously recorded Type B neurons (respectively, n=11 pairs). **(C)** We made simultaneous current clamp (CC) recordings from a fast-spiking interneuron (FSIN, green) and voltage clamp recordings from either a Type A or B neuron. Current was injected to elicit FSIN spiking while recording from the pyramidal neuron in voltage clamp at +10 mV (VC10). **(D)** The connection probability from FSINs was greater onto Type A neurons than Type B neurons (n=23 pairs).**(E)** Experimental design: We recorded simultaneously from a Type A and B neuron in PV::Cre mice injected with virus to drive Cre-dependent ChR2-EYFP expression (yellow, left). During optogenetic stimulation of ChR2-expressing PV interneurons, we recorded simultaneous IPSCs in Type A and B neurons (bottom right). **(F)** PV interneuron-mediated IPSC peak amplitude (left) and inhibitory charge transfer (right) were greater in Type A than Type B neurons (n=5 pairs). **(G)** Normalized, averaged EPSPs in Type A and B neurons following optogenetic stimulation of callosal inputs. Type A neurons (red) repolarize faster (arrow marks repolarization).**(H)** The decay time constant of callosally-evoked EPSPs is faster in Type A neurons (n=11 pairs). See also Fig. S4.